Science of the Total Environment xxx (xxxx) xxx

Contents lists available at ScienceDirect

Science of the Total Environment

journal homepage: www.elsevier.com/locate/scitotenv

Time-dependent molecular progression and acute toxicity of oil-soluble, interfacially-active, and water-soluble species reveals their rapid formation in the photodegradation of Macondo Well Oil

Huan Chen [a,*], Amy M. McKenna [a,c], Sydney F. Niles [a,b], Joseph W. Frye [a,b], Taylor J. Glattke [a,b], Ryan P. Rodgers [a,b,*]

[a] National High Magnetic Field Laboratory, Florida State University, 1800 East Paul Dirac Dr., Tallahassee, FL 32310, USA
[b] Department of Chemistry and Biochemistry, 95 Chieftan Way, Florida State University, Tallahassee, FL 32306, USA
[c] Department of Soil and Crop Sciences, Colorado State University, 1170 Campus Delivery, Fort Collins, CO 80523, USA

HIGHLIGHTS

- Photoproducts of MWO from 1 h to 120 h of 3 fractions were tracked by FT-ICR MS.
- Rapid oxidation and increased toxicity were observed in <24 h irradiation periods.
- Oxygenated N and S containing photoproducts increased with irradiation time.
- The study depicts molecular temporal evolution of photooxidation progression.

GRAPHICAL ABSTRACT

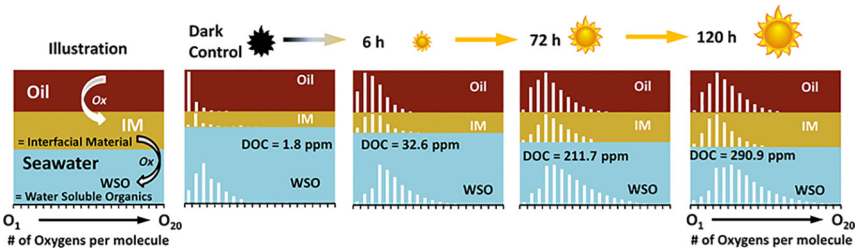

ARTICLE INFO

Article history:
Received 7 October 2021
Received in revised form 15 November 2021
Accepted 18 November 2021
Available online xxxx

Editor: Jay Gan

Keywords:
Deepwater Horizon oil spill
Photooxidation
Solar simulation
Microtox®
Acute toxicity
FT-ICR MS

ABSTRACT

Photodegradation is a significant weathering process that transforms spilled oil, yet, the fate, degradation rate, and molecular transformations that occur through photoinduced pathways remain relatively unknown. The molecular complexity combined with the increased polarity of photoproducts challenges conventional analytical techniques. Here, we catalogue the molecular progression of photochemical transformation products of Macondo Well Oil by negative-ion electrospray ionization (ESI) Fourier transform ion cyclotron resonance mass spectrometry (FT-ICR MS). We track the molecular compositions of oil-soluble, interfacially-active, and water-soluble oil species formed at varying time intervals in photomicrocosm experiments. Short photoirradiation periods (<24 h), not previously reported, are included to reveal rapid photooxidation of native oil components. Surface oil films exposed to solar irradiation were shown to increasingly contribute to the dissolved organic carbon pool as a function of increased irradiation time. FT-ICR MS analysis of acidic species of each fraction identifies tens of thousands of oil-soluble, interfacially-active, and water-soluble phototransformation products, including O_x, NO_x, and SO_x species. Oil-soluble species incorporate oxygen as a function of irradiation periods. After 96 h of irradiation, ~14 wt% of the photooxidized oil film was interfacially active and contained phototransformed species with up to 12 oxygen atoms per molecule. Water-soluble species correspond to highly oxygenated compounds. Importantly, photochemical oxidation is shown to occur within the first hour. Beyond 24 h, photoproducts remain compositionally similar, highlighting the rapid effect of photodegradation to transform oil species into water-soluble compounds. Molecular fingerprints provided by FT-ICR MS highlight the oxygen dependence on oil/water solubility. Microtox® analysis indicates that the toxicity of water-soluble photoproducts rapidly increases at early irradiation time points (first 24 h) compared to the dark control and reaches a maximum at 6 h of irradiation. Results highlight the temporal, molecular progression of photoproducts as they partition from oil-soluble to oil-soluble interfacially-active, and finally to water-soluble species.

* Corresponding authors at: National High Magnetic Field Laboratory, Florida State University, 1800 East Paul Dirac Dr., Tallahassee, FL 32310, USA.
E-mail addresses: huan.chen@magnet.fsu.edu (H. Chen), rodgers@magnet.fsu.edu (R.P. Rodgers).

http://dx.doi.org/10.1016/j.scitotenv.2021.151884
0048-9697/© 2021 Elsevier B.V. All rights reserved.

Please cite this article as: H. Chen, A.M. McKenna, S.F. Niles, et al., Time-dependent molecular progression and acute toxicity of oil-soluble, interfac..., Science of the Total Environment, http://dx.doi.org/10.1016/j.scitotenv.2021.151884

1. Introduction

The 2010 Deepwater Horizon (DWH) disaster prompted an immense investment in oil spill-related research that has reshaped the traditional understanding of the photochemical weathering process at the sea surface (Ward and Overton, 2020; Bacosa et al., 2015; Ward et al., 2018; Kujawinski et al., 2020; King et al., 2014). These studies have shown that once released, oil molecules undergo biotic and abiotic modifications that dictate the transport, fate, water-solubility, bioavailability, and toxicity of native oil. Despite numerous physical weathering processes (e.g., evaporation, dissolution), which may enhance oil emulsification and increase the concentration of naturally occurring surfactants, they alone cannot account for the massive amounts of emulsions and mousses observed in the field after the oil spill (Lewan et al., 2014; Stout et al., 2016). Thus, recent research has suggested that these species that interact strongly with water to form emulsions are generated in situ through chemical processes such as photooxidation (Ward et al., 2018; Passow and Overton, 2021).

Past research established photochemical oxidation as a significant weathering process that removes spilled oil from the biosphere and is implicated as an important oil degradation process, as documented by oil spill studies over past decades (Garrett et al., 1998; Dutta and Haryama, 2000; Guipeng et al., 2006; Ali et al., 1995; Fernandez-Varela et al., 2006; Maki et al., 2001). Such studies relegate photodegradation to a secondary, slow process that occurs over several days to weeks after a spill (Ward and Overton, 2020), despite early studies that suggested photooxidation forms surface-active, oil-soluble compounds and could be the primary pathway for the formation of surface emulsions (Thingstad and Pengerud, 1983). Recent studies confirm that photooxidation generates oil-soluble, oxidized species that contribute to emulsion formation on the sea surface (Stout et al., 2016; Niles et al., 2019; Radović et al., 2014). However, the rate of formation, transformation products, and the long-term fate of highly polar oil-derived photoproducts remain largely undetermined (Zhou et al., 2013; Harriman et al., 2017). A possible explanation for this knowledge gap may be due to the inherent high complexity of crude oil, and the fact that sunlight further increases this complexity through the production of polyfunctional, oxygen-rich transformation products over time.

The sum of molecular complexity, combined with the increased range of molecular polarities of the photoproducts, precludes analysis by conventional chromatographic techniques (Gough and Rowland, 1990; Aeppli et al., 2012; Gros et al., 2014). However, advances in Fourier transform ion cyclotron resonance mass spectrometry (FT-ICR MS) provide insight into chemically complex environmental transformation products at the molecular level without boiling point limitations (Ruddy et al., 2014; Corilo et al., 2013; Seidel et al., 2016; McKenna et al., 2013). Recent work has demonstrated the capability of FT-ICR MS to identify tens of thousands of oxidized transformation products in weathered oil derived from the DWH oil spill (Niles et al., 2019; Chen et al., 2016; Vaughan et al., 2016; Zito et al., 2020; Radović et al., 2020; Niles et al., 2020a). Because oil degradation occurs through multiple potential pathways, photoirradiation-only microcosm experiments combined with FT-ICR MS were used to reveal the photooxidation products of the BP supplied surrogate Macondo Well Oil (MWO). The work suggested a link between the transition of initially hydrophobic native oil species into oxidized, water-soluble species through an intermediate state, partially oxidized interfacially-active photoproducts (Zito et al., 2020). Still, the study was limited to one 24 h timepoint. A previous study reported differences in compound class distributions between surrogate oil and MWO after photochemical alterations (Vaughan et al., 2016). Laboratory microcosm studies indicate that compared to biodegradation, photooxidation is the initial dominant mechanism to produce oil-soluble transformation products, which resemble the ketone/aldehyde species in field samples, and investigated the progression of sulfur-containing compounds into oil and water-soluble photoproducts (Niles et al., 2019, 2020a). The importance of photooxidation is now well recognized, but the detailed molecular-level understanding, especially how it progresses as a function of time, is currently unknown. Additionally, there have been conflicting reports as to the toxicity of phototransformed hydrocarbons (King et al., 2014; Barron, 2017; Zito et al., 2019).

Solar radiation absorbed by polycyclic aromatic hydrocarbon (PAH) chromophores can produce free radicals that react with oxygen to produce reactive species that can damage DNA and other cellular macromolecules (Lee, 2003). Previous studies suggest that newly-formed oxygenated hydrocarbons from photooxidation are more toxic than the precursor compounds (Barron et al., 2003; Lelario et al., 2021). In contrast, studies of oiled Artic sediment (Lee et al., 2003) and weathering of surface slicks (Echols et al., 2015; Faksness et al., 2015) suggest a rapid decrease of toxicity during weathering. Previous studies (Zito et al., 2019) report water-soluble species formed through photooxidation of a surrogate Macondo oil (provided by BP August 2011) had increased toxicity after 24 h that decreased with extended exposure. This suggests that sunlight induces rapid (less than 24 h) molecular changes that increase toxicity, and molecular identification of these transformations is essential to assess the impact of photochemical oil degradation on surrounding ecosystems. Thus, here, we track photogenerated acidic oil species via photodegradation from 1 h to 120 h for all 3 of the previously identified fractions: oil-soluble, oil-soluble but interfacially-active, and finally, water-soluble species. The analysis utilizes both negative-ion (−) electrospray ionization (ESI) FT-ICR MS to track changes in molecular compositions of both oil- and water-soluble acidic species and Microtox® toxicity assays to determine potential adverse environmental impacts for each MWO photomicrocosm time point.

2. Materials and methods

2.1. Photooxidation microcosm

All solvents were HPLC grade (JT Baker, Phillipsburg, NJ). Macondo Well Oil (obtained as standard reference material SRM 2779) was purchased from the National Institute of Standards and Technology (NIST, Gaithersburg, MD) (Murray et al., 2016). MWO oil was collected from the leaking Macondo well during the Deepwater Horizon oil spill as previously reported (Murray et al., 2016). Photochemical microcosms were performed by dispensing 325 mg (385 μL) of MWO to 50 mL autoclave-sterilized 70% artificial seawater (Instant Ocean Aquarium Systems, Inc., Mentor, OH, USA) as previously described (Niles et al., 2019; Zito et al., 2020), to generate ~120 μm oil film in a 250 mL jacketed beaker attached to a water chiller to ensure a constant temperature of 27 °C. All glassware was acid washed and precombusted in a muffle furnace (550 °C for 4 h) prior to use.

2.2. Solar simulation

Microcosms were placed in a solar simulator (Atlas Suntest CPS + (II), AMETEK) and subjected to artificial sunlight for discrete irradiation periods (1, 3, 6, 12, 18, 24, 48, 72, 96, and 120 h). The solar irradiance is set at 765 W/m^2, which was roughly equivalent to 4 days of natural sunlight in the Gulf of Mexico per 24 h of photoirradiation in the solar simulator (Zito et al., 2019; Roebuck et al., 2017). A dark control was established by wrapping the beaker containing the same amount of water and oil with aluminum foil to prevent light exposure and stirring for 120 h for comparison with the irradiated samples. The dark control is denoted as 0 h in figures and data interpretation.

2.3. Extraction of oil, IM, and WSO

2.3.1. Isolation of oil-soluble species

After each irradiation period, the water layer of the microcosm was transferred to a glass container by glass pipets for water-soluble organics (WSO) extraction. The oil layer was left in the beaker and removed by rinsing with toluene, transferred to a pre-weighed vial, and desolvated under dry nitrogen gas.

2.3.2. Isolation of interfacial material (IM)

IM was isolated from ~80 mg of irradiated oil of each timepoint based on the wet silica method (Jarvis et al., 2015; Clingenpeel et al., 2015) to isolate interfacially-active species that remain in the oil layer. After separation, the dried oil and IM were stored under argon gas prior to analysis to prevent further oxidation.

2.3.3. Isolation of water-soluble organics

Water from each time point was removed from the microcosm with a glass pipet and filtered through a 0.45 μm nylon filter to remove undissolved oil. Approximately 20 mL of filtered water was acidified to pH 2 with trace-metal free HCl, followed by solid-phase extraction (SPE) with styrene-divinylbenzene (SDVB) polymer modified with a proprietary nonpolar surface (Bond Elute Priority Pollutant™, Agilent Technologies) (Dittmar et al., 2008). Briefly, acidified samples were loaded onto an SPE cartridge followed by elution with methanol. A 10 mL aliquot of each water sample was reserved for dissolved organic carbon (DOC) quantification, and a 4 mL aliquot of each water sample was saved for Microtox® acute toxicity analysis. All samples were stored in precombusted glass vials at 4 °C in the dark prior to downstream analyses.

2.4. DOC measurement

DOC concentrations were measured with a Shimadzu total organic carbon (TOC-V WS) analyzer. Each sample was diluted with deionized water (10 mL sample + 30 mL water). Samples were acidified to pH 2 using H_3PO_4, with 3% acid injection for each sample. Sodium persulfate (1.5%) was injected as the UV oxidizing agent. The sample concentrations were determined using a six-point calibration curve between 0 and 50 ppm (0, 1, 5, 10, 20, and 50) from a 1000 ppm Organic Carbon stock solution. The auto dilution feature on the TOC analyzer was enabled to ensure the samples were within the calibration curve. The acidified samples (pH 2) were sparged for 3 min to remove inorganic carbon. The mean of three injections of 6 mL is recorded for every sample, and the coefficient of variance (CV) was within 2% for replicate injections.

2.5. Acute toxicity analysis

Microtox® toxicity analysis (Brohon et al., 2001; Morales-Caselles et al., 2007; Pelletier et al., 2004) was used to track the toxicity of water-soluble petroleum transformation products collected at different time periods. Water samples from both test and control microcosms were carbon normalized to 20 ppm of C based on DOC values prior to Microtox® testing. Dark control and 1 h irradiated sample were preconcentrated to 10 ppm, and 3 h irradiated sample was concentrated to 20 ppm of C. The decrease in the bioluminescence of *Alivibrio fischeri* bacteria after a 15 min incubation period establishes toxicity of each water fraction through measurement of light emitted by the bacteria. The Microtox® 81.9% screening test protocol was used on the Microtox® model 500 analyzer (Modern Water, New Castle, DE, USA) as described by Zito et al. (2019). In this study, the toxicities of short irradiation periods within the first 24 h were included in the series.

2.6. Negative-ion 9.4 Tesla FT-ICR mass spectrometry

Each oil sample was dissolved in toluene (1 mg/mL) that was further diluted to 250 μg/mL in 50:50 toluene/methanol (MeOH) (by volume). IM fractions were reconstituted in dichloromethane (DCM) and further diluted to 250 μg/mL in 50:50 DCM/MeOH. WSO concentrations were adjusted with MeOH to a final concentration of 100 μg of C/mL without additional modification. Oil and IM samples were spiked with 0.125% (by volume) tetramethylammonium hydroxide (TMAH, 25% by weight in MeOH) to facilitate deprotonation (Lobodin et al., 2013). Samples were analyzed on a custom-built FT-ICR MS equipped with a 9.4 Tesla superconducting solenoid magnet, as previously reported (Ruddy et al., 2014; Corilo et al., 2013; McKenna et al., 2013; Kaiser et al., 2011; Chen et al., 2018). Complete experimental methods, FT-ICR MS instrumentation parameters, and data processing are provided in the Supporting Information.

3. Results and discussion

3.1. DOC concentrations increase rapidly as a function of solar exposure time

Fig. 1 shows the dissolved organic concentration (DOC, left, red circles) and acute toxicity per unit carbon (right, green squares) versus

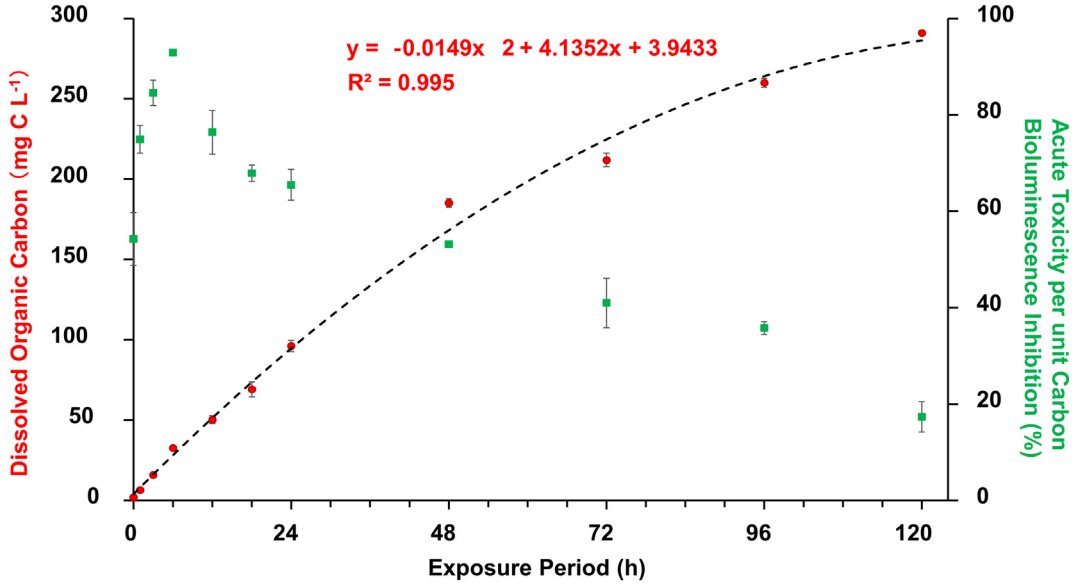

Fig. 1. DOC photoproduction (red dot) and 15 min bioluminescence inhibition (green square) of MWO water-soluble organics (WSO) over time. A quadratic increase in the DOC concentration with extended solar exposure is shown with the dashed black trendline (r^2 = 0.995), which highlights the temporal differences in the rate of DOC production. Bars indicate the standard deviation of triplicate measurements. (For interpretation of the references to colour in this figure legend, the reader is referred to the web version of this article.)

photoirradiation time for water-soluble fractions from irradiated oil with error bars indicating the standard deviation of triplicate measurements. During the first hour of photodegradation, the DOC increased by more than a factor of 3, from 1.8 mg carbon/l (C/L) (dark, 0 h) to 6.3 mg C/L (1 h irradiation), as demonstrated by the red circles. By 24 h of irradiation, the C/L values rapidly increased to ~100 mg, more than 1/3 of the total DOC produced in the 120 h irradiation period (290.0 mg C/L) (Fig. 1, Table S1). Temporal differences in the rate of DOC production are highlighted by the quality of the quadratic fit for 0 and 6 h, 6 and 48 h, and 48 and 72 h, and suggest that the rate of DOC production decreases from its initial rate as a function of irradiation period. Previous reports with BP surrogate MWO report a DOC concentration of 189.9 mg C/L after 120 h of solar exposure (Zito et al., 2019); however, MWO obtained as NIST SRM 2779 shows nearly 1.5-fold higher DOC concentration for the same exposure time, which is in agreement with previous reports that highlight photochemical differences between MWO and the BP supplied surrogate oil (Vaughan et al., 2016).

3.2. Acute toxicity as a function of irradiation period

The WSO produced from the irradiations of MWO for each time point were analyzed for acute toxicity per unit carbon by Microtox® to evaluate toxicity as a function of sample composition (rather than concentration, which was held constant). The trend seen for the acute toxicity per unit carbon in Fig. 1 (green squares) agrees with previous reports for the same periods: it demonstrates elevated toxicity at 24 h relative to the dark control, followed by a steady decrease over time, although time points within the first 24 h were not measured (Zito et al., 2019). Here, we confirm previous reports of increased toxicity at 24 h (Zito et al., 2019), but quantify the rapid phototransformation (DOC production) that occurs within the first 24 h (1 h, 3 h, 6 h, 12 h, 24 h) and explore its relationship to increased toxicity. Notably, the acute toxicity of WSO per unit carbon increased from 54% at $t = 0$ to 76% after only 1 h of photoirradiation. The toxicity peaked at 92% after 6 h of solar exposure (1–2 days solar equivalent) then rapidly decreased in the 6–24 h time periods, although the 24 h toxicity remains elevated compared to that of the dark control (similar to that previously reported with the surrogate oil) (Zito et al., 2019). The toxicity then gradually decreased to 17% at 120 h of exposure (30 days solar equivalent). Despite carbon normalization for all toxicity tests, the data suggests that photooxidation products derived from MWO oil films are most toxic within the first 6 h of solar exposure when the rate of DOC production is at a maximum and at longer irradiation times (>48 h), where the DOC production rate is at a minimum, the toxicity is lower relative to the dark control. Whether this suggests that direct photooxidation products that might form preferentially at early irradiation periods are responsible for the increased toxicity is currently unknown, but differences in water-soluble molecular compositions are discussed below.

3.3. The photooxidation compositional continuum with increased solar irradiation time

Previous work demonstrated that the solar irradiation of the Macondo surrogate oil resulted in tens of thousands of photoproducts that span a wide range of solubilities which include: oil-soluble, oil-soluble but interfacially-active, and water-soluble compounds (Zito et al., 2020). In the study using surrogate MWO, photooxidized transformation products identified by (−) ESI FT-ICR MS were shown to progress step-wise from oil-soluble to interfacially active (oil-soluble) to water-soluble species as a function of carbon number and oxygen content. However, the surrogate oil was analyzed for only a single (24 h) irradiation period (Zito et al., 2020). Our work includes 10 irradiation periods and reveals that this progression process is time-dependent. From Fig. 1, we understand that toxicity and DOC rates exhibit non-linear trends, which would not be understood without short irradiation periods in the first 24 h, and thus we examine the process of IM and water-soluble production as a function of both short and long solar irradiation times (1 − 120 h).

Because FT-ICR MS yields elemental composition assignments for tens of thousands of peaks (i.e., individual compounds) in a single mass spectrum, van Krevelen diagrams provide rapid visualization of large volumes of molecular ions detected by ultrahigh-resolution mass spectrometry to highlight compositional differences between samples (Kim et al., 2003). A plot of the H/C versus O/C for all elemental compositions identified in the analysis of the oil-soluble, oil-soluble IM, and WSO at each irradiation time point is shown in Fig. 2. The photoproducts span a wide range of H/C ratios (0.5–2.0) and O/C ratios (0.1–0.9), with a marked increase in the O/C ratio for water-soluble photoproducts. Thus, since FT-ICR MS provides elemental composition assignment for each mass spectral peak, relative abundance-weighted average O/C values (O/C_{aw}, red arrows, Fig. 2) are calculated for each plot (Sleighter and Hatcher, 2008).

3.4. Compositional trends for the oil-soluble species

Photooxidation of MWO generates various highly-oxidized species, a portion of which remains oil-soluble even after extensive irradiation. These species become more oxidized with increased solar exposure; within the first hour, the O/C_{aw} doubles from 0.04 at 0 h to 0.08 and subsequently increases to 0.18 at 120 h (Fig. 2a). The carbon number range of the oil-soluble species remains relatively constant as a function of increased irradiation time (highlighted later). Therefore the increase in the O/C_{aw} is a consequence of increasing oxygen content. Fig. S1 captures this temporal evolution in the heteroatom class distribution for O_x, O_xS_1, and N_1O_x species derived from (−) ESI FT-ICR MS for oil-soluble species from the photooxidation microcosms. The top panel of Fig. S1 demonstrates that for the dark control (0 h), the most abundant O_x species are in the O_1 class, which could correspond to phenols, alcohols, or aldehyde/ketone

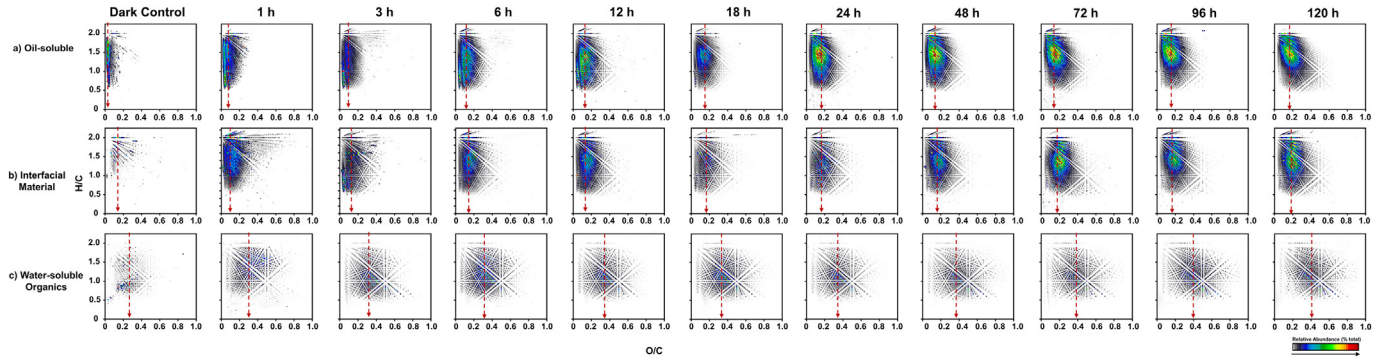

Fig. 2. Van Krevelen diagrams of the acidic oxygenated species from lab irradiated MWO oil identified by (−) ESI FT-ICR MS. Dashed lines arrows denote the abundance weighted average O/C ratio for the oil-soluble, IM, and WSO generated under various solar exposure periods. (For interpretation of the references to colour in this figure, the reader is referred to the web version of this article.)

intermediates (McKenna et al., 2013). This observation agrees with reports for the parent MWO, which contained less than 2% relative abundance of higher oxygen classes (O_2–O_5) before irradiation (Reddy et al., 2011). After 3 h of irradiation, the most abundant compound class is O_2, which most likely is comprised of high amounts of carboxylic acids. After 6 h, O_2–O_6 classes present with increased relative abundance (8%), which further increases after 12 h (up to 12%). The oxidation of oil-soluble species is monitored to 120 h (equivalent to 30 days), revealing the continued trend in the increased relative abundances of higher-order oxygen-containing species. Importantly, it also reveals that the largest increase in oxygen content occurred in the first 24 h of irradiation. Between 0 and 24 h, the oil-soluble photoproducts rapidly increase in oxygen content and relative abundance to nearly match that of the later time periods (apex at O_4 and range of O_1–O_{12}). Such a rapid increase is notable and not captured in previous studies.

3.5. Temporal evolution of Ox photoproducts

3.5.1. Oil-soluble species

Fig. S2 shows isoabundance-contoured plots of double-bond equivalents (DBE) versus carbon number for the oil-soluble Ox classes derived from (−) ESI FT-ICR mass spectra for each time point from the solar simulation microcosms. Oxygenated species in the oil-soluble fraction present across a wide range of carbon numbers, from 8 carbons to over 70 carbons, and a shift to higher carbon number is observed as oxygen content increases. For example, after 1 h, oil-soluble species with 1 to 5 oxygen atoms (O1–O5 class) and up to 45 carbon atoms were observed. Furthermore, for more extended irradiation periods (18 h to 120 h), the presence of photoproducts that extend to C_{70} is observed in higher-oxygenated species (e.g., O_9). A recent study reports the increase of compounds with low molecular weight and the number of oxygen atoms of an Italian crude oil after one week of solar irradiation under a xenon lamp. In addition, the study observed the increase in unsaturation in the irradiated oil, thus assuming higher toxicity for the oil after irradiation (Lelario et al., 2021). However, in our irradiation experiments with MWO, the DBE versus carbon number plots from longer irradiation periods (18 h–120 h) exhibit remarkable resemblance to each other for a given O_x class, suggesting that the molecular composition of oil-soluble photoproducts does not change dramatically with longer irradiation periods (greater than 12 h).

Furthermore, photoproducts span a wide range of aromaticity (DBE values = 1–25), which suggests both indirect and direct photooxidation occurs in the oil-soluble fraction. Direct photooxidation occurs when polyaromatic compounds (DBE > 7) absorb light to produce reactive transient species such as singlet oxygen and hydroxyl radicals that can either lead to oxidation of the chromophore (direct oxidation) or subsequent oxidation of compounds that lack a chromophore, such as alkanes/cycloalkanes (indirect photooxidation) (Vione et al., 2014). Thus, the presence of low-DBE photoproducts (which lack a chromophore) suggests indirect photooxidation of saturates may occur. In the O_1 class, the phenol/alcohols comprise highly aromatic, condensed ring systems that likely serve as photochemical intermediates for direct photooxidation; hydroxyl radical is most likely responsible for alkane oxidation since singlet oxygen does not react with saturated hydrocarbons (Ray and Tarr, 2014). Singlet oxygen can react with aromatic rings, typically forming aldehyde and ketone products that can be further oxidized to acids. As previously reported, fluorene hydrocarbons (DBE 9–12) were highly abundant in parent MWO and could serve as the precursor for the highly aromatic O_1 species (McKenna et al., 2013). The formation of carboxylic acid classes (O_2 and higher) requires multiple oxidation steps (i.e., aromatics react with hydroxyl radicals to produce alcohols or carbonyls, which subsequently generate ring-opening photoproducts) (Ray and Tarr, 2014).

3.5.2. Interfacially-active species

Photooxidation of surface oil also forms IM, surfactant-like species that facilitate the transition of oil-soluble to water-soluble compounds. After extensive photooxidation, the transformation products become more polar, which in turn increases their interaction with water (interfacial activity). The composition of the IM layer is illustrated by the H/C versus O/C plots in Fig. 2b; the IM exhibits H/C and O/C values that lie between those of oil-soluble and water-soluble species with a notable overlap with that of the oil-soluble species (discussed later). These interfacially-active species promote the trapping of water by the photooxidized oils and, therefore, have a profound effect on the physical and chemical properties of the weathered oil. This phenomenon is consistent with the observation of high viscosity mousses observed in the field following oil spills (Lewan et al., 2014; Daling et al., 2014).

Isolation of IM from oil followed by FT-ICR MS analysis provides unique molecular insight into its composition (Jarvis et al., 2015; Clingenpeel et al., 2015; Lalli et al., 2017). Fig. S3 shows the amount of IM isolated from 80 mg of irradiated oil for each microcosm irradiation period (bottom panel) along with the corresponding % weight in the table (top panel). Without solar irradiation (dark control, $t = 0$ h) and equivalent stirring, ~1.5 mg of IM was collected, and no emulsification was observed. However, after 6 h, the IM mass increased to 2.4 mg, and at 24 h, the mass of IM recovered had doubled from the dark control value (to 3.2 mg after 24 h). From 24 to 48 h, another two-fold increase in IM mass occurs (6.5 mg) up until 72 h (10.9 mg), where IM generation slightly decreases between 96 h (10.9 mg) and 120 h (9.7 mg). Decreased IM yield in the longest irradiation period could be due to the transfer of highly-oxygenated material to the water layer; as Fig. 2 illustrated, once a molecule reaches an O/C greater than ~0.4–0.5, it is transferred from the IM layer to the water.

Previous studies found that interfacially-active species in Athabasca Bitumen oil comprise less than 1% by weight but are solely responsible for stable emulsion formation (Clingenpeel et al., 2015). Visual inspection of the photomicrocosms after 0 h, 1 h, and 3 h of solar irradiation suggests that sunlight is responsible for the formation of surface emulsions, which are present after 1 h of irradiation, whereas the dark control shows no emulsification after 120 h of mixing. These observations are consistent with the IM yields reported in Fig. S3, which suggest that the emulsion-forming behavior observed is due to increased IM content, and after 96 h irradiation, ~14 wt% of photooxidized film was interfacially-active (Fig. S3 inset). Fig. S4 shows the heteroatom class distribution for interfacially-active acidic species (O_x, O_xS_1, and N_1O_x) for each irradiation period. For all irradiation periods (1 h–120 h), IM species are enriched in oxygen across both nitrogen- and sulfur-containing classes relative to the dark control (0 h, black).

3.5.3. Water-soluble organics (WSO)

Due to increased photooxidation, and therefore increased polarity, oil molecules move from oil-soluble to IM and finally to WSO with an increasing O/C ratio. Fig. S5 shows the heteroatom class graph for acidic WSO species formed through irradiation and demonstrates the presence of highly oxidized transformation products (e.g., O_{15}, $O_{10}S_1$, and N_1O_{10}).

Recent work reports the formation of water-soluble oxygenated hydrocarbons from asphalt following solar irradiation and shows that increased irradiation time produces higher-order oxygenated compounds and higher DOC content (Niles et al., 2020b). The WSO fraction is the most oxidized, which is demonstrated by the highest average O/C ratio among the three solubility fractions for the same irradiation time point (Fig. 2). The WSO O/C ratio increased from 0.25 at 0 h to 0.41 at 120 h, which compared to the other two fractions with the O/C ratios <0.2 at 120 h, is the highest increase in the three fractions. The differences in O/C ratios for the WSO and oil-soluble fractions are dramatic (Fig. 2).

As discussed earlier, the water-soluble species formed in the first 6 h of irradiation were generated rapidly and demonstrated significantly higher toxicity than those generated after longer irradiation periods. Those that formed between 6 and 12 h formed slightly slower based on the DOC measurements but still exhibited higher toxicity than that of the dark control (Fig. 1). Previous Microtox analysis has shown that toxicity and the ring structure of polyaromatic hydrocarbons (PAHs) tended to correlate as PAHs with fewer ring numbers are more toxic (Johnson, 2018). Unfortunately, a comparison of the van Krevelen diagrams of the water-soluble

species (Fig. 2c) doesn't show dramatic differences between the O/C and H/C patterns as a function of the increased irradiation period. Only slight differences are discernable in the low (O/C < 0.4) oxygen species with H/C ratios between 0.5 and 1.5. Thus the temporal differences in toxicity are potentially due to differences in carbon number (not captured in the van Krevelen plot, discussed below) or in oxygen chemical functionality, which is difficult to determine in these polyoxygenated photoproducts.

3.6. Carbon number dependence of interfacial activity and photoproduct solubility

Fig. 3 shows the O/C ratio versus carbon number distribution for O_x species for oil-soluble, IM, and WSO fractions for 0, 1, 18, and 120 h irradiation periods. Comparison of the 3 panels in each column reveals the relationship between carbon number, and degree of oxidation (O/C) that determines the solubility layer location (oil, IM, or water) of a compound. Starting at the dark control (0 h), oil-soluble species with no interfacial activity (top left panel) span the widest carbon number distribution ($10 < C < 80$) with the fewest oxygen atoms per molecule (ranging from O_1–O_3, with an $O/C < 0.2$). Interfacially-active, oil-soluble species from the dark control have slightly higher oxygen content (from O_1–O_5) but exhibit a dramatically compressed carbon number range ($10 < C < 30$), which results in an increase in the maximum O/C ($O/C < 0.6$). Water-soluble species extracted from the dark control share a similar carbon range as the IM, but with increased oxygen content (from O_1–O_{10}).

As photooxidation progresses for the oil-soluble species (1, 18, and 120 h), the carbon number remains relatively constant, but the O/C ratio increases steadily to a maximum of 0.7. However, the most abundant oil-soluble photoproducts remain below an $O/C < 0.4$, as seen in the 120 h oil-soluble photoproducts plot. IM and water-soluble species exhibit differing extents of oxidation, but similar carbon number ranges that widen with increased irradiation times and are also compressed relative to the oil-soluble species. Thus, the large compositional overlap between oil solubles and IM (noted earlier in Fig. 2) is a combination of increasing oxygen content and concurrent changes in carbon number that result in overlapping H/C and O/C ratios, irrespective of structural and chemical functionality differences. The most obvious example of the oxygen/carbon number dependence on partitioning is shown for the 120 h irradiation period, where due to the hydrophobicity of higher carbon number species, a void exists in the continuum of water-soluble species O/C vs. carbon number plot (bottom right plot, highlighted by red arrows). Conversely, the IM fraction from 120 h irradiation contains an O_x distribution ($O_1 - O_{12}$) that overlaps with that of the oil-soluble species ($O_1 - O_{14}$, Fig. 3, top, right), but each oxygen class in the overlapped classes have different carbon number ranges. Water solubility has imposed strict restrictions on carbon number and O/C values: species with low carbon number require fewer oxygen atoms to achieve an O/C ratio that allows them to dissolve in water. Additionally, we observe that as irradiation time increases, oxygen content and carbon number both increase. For example, at 0 h, water-soluble species have up to 10 oxygen atoms and fewer than 40 carbon atoms. However, as the irradiation period increases to 120 h, compounds with up to 20 oxygen atoms are observed, and the carbon number increases to over 50. This observation supports the theory that compounds with higher carbon number require a higher number of oxygens per molecule to make the photoproducts water-soluble. The narrow carbon number distribution of the WSO's after 1 h of irradiation widens slightly in the 18 h irradiation and continues to widen as the irradiation period increases to 120 h. Many species that are present in the water-soluble extract for 120 h are also present in the other WSO fractions; this observation suggests that the carbon number and O/C ranges do not affect the toxicity of photoproducts. Thus, as previously discussed, the structure and/or chemical functionality of the early period photoproducts are most likely the source of increased toxicity.

3.7. Molecular-level summary of photodegradation of oil

Fig. 4 displays the molecular oxygen content relative abundances of oxygenated species and thus depicts compositional changes as the MWO photochemically degrades over time and reveals the temporal progression of O_x compositional changes in oil-soluble, IM, and WSO fractions. It shows how progressive oxidation could affect the chemical/physical behavior through

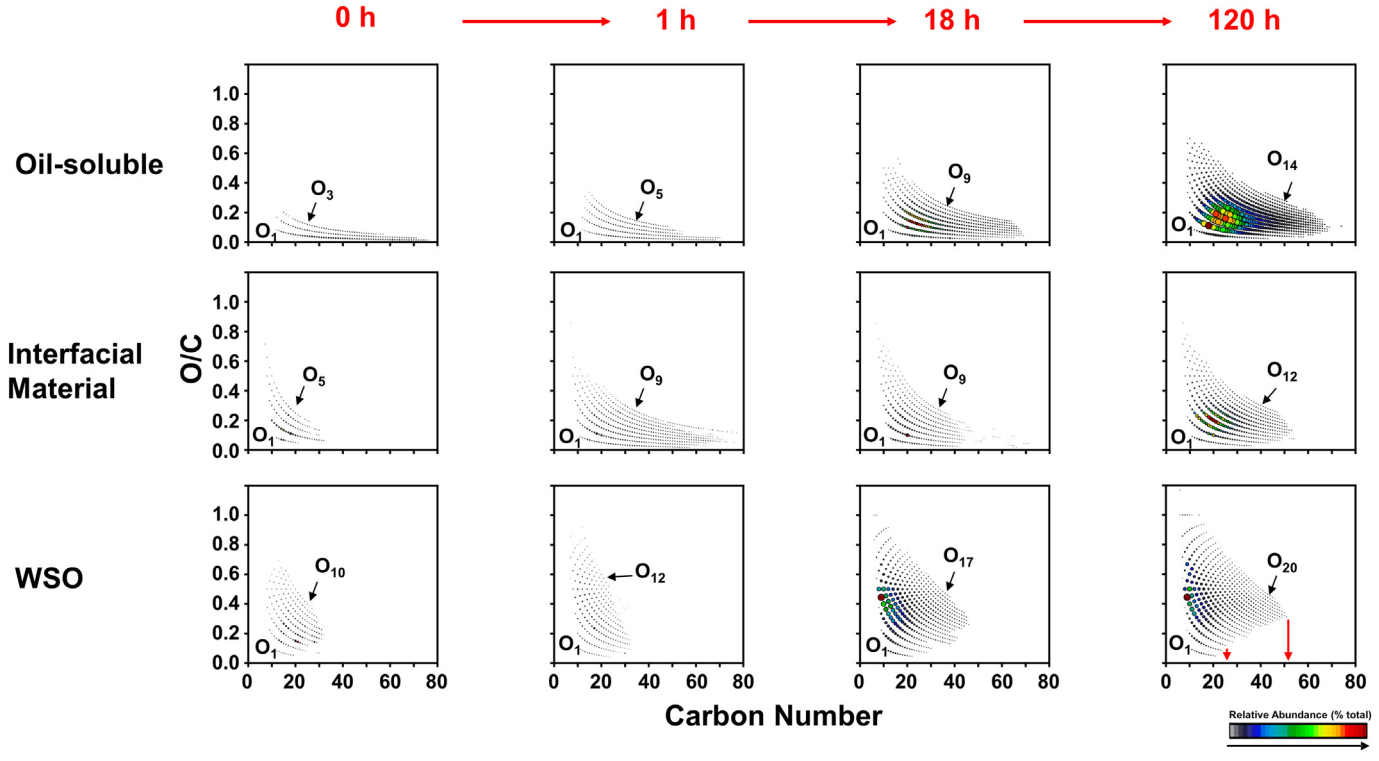

Fig. 3. O/C ratio vs. carbon number plots identifying the dependence of O_x species derived from (−) ESI FT-ICR MS on oil/water partitioning behavior in microcosm irradiated at 0 h, 1 h, 18 h, and 120 h. The oxygen class range is included for all samples presented.

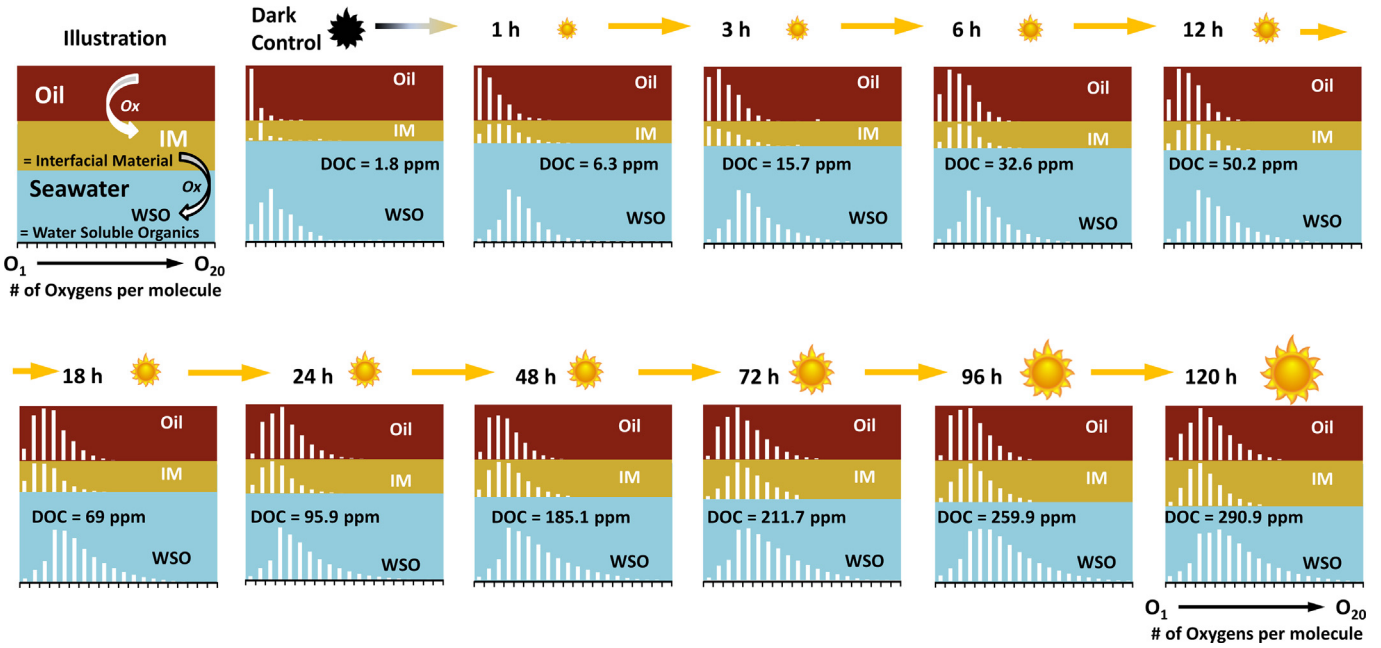

Fig. 4. Schematic summary of solar simulation microcosms depicting the temporal progression of O_x revealed by FT-ICR MS. X-axis exhibits the molecular oxygen content (O_1–O_{20}), and the y-axis shows the relative abundance of these oxygenated species. The dark control serves as a $t = 0$ marker for the subsequent monitoring of photo transformation products.

the generation of IM, which partitions to the oil/water interface. Specifically, the partitioning of O_x species from oil to water appears to be mediated by interfacially active species. In the dark control microcosm, the IM is comprised of low abundance, native oil surfactants, centered at O_2 species (typically naphthenic acids). As photooxidation in the oil fraction begins (e.g., at 1 h), higher-order oil-soluble oxygenated species are generated, some of which are interfacially active. Extensive photoirradiation (e.g., at 120 h) increases and broadens the oxygen content distributions for the oil-soluble and IM species and produces compounds with up to 20 oxygen atoms in the water-soluble fraction. The DOC values, which represent the amount of dissolved carbon in the WSO fraction, demonstrates that photooxidized oil contributes to the dissolved organic carbon pool as early as 1 h of irradiation. This process appears to occur in a step-wise fashion, where oxidation of oil-soluble species generates an increasing mass fraction of IM (Fig. S3), and further oxidation of IM yields WSO. This is illustrated by the increasing DOC values as a function of irradiation time. Additionally, the number of oxygen atoms per molecule also increases (white bars in Fig. 4) with the irradiation period. The number of oxygen atoms per molecule increases in all three fractions (oil, IM, and WSO) with extended exposure time, indicating that native species initially present in the starting material are further oxidized upon solar irradiation. The extent of oxygenation is correlated with the shift from oil-soluble to IM and from IM to water-soluble as a function of time.

3.8. The SO_x and NO_x continua

In addition to the O_x species, increased abundances of oxygenated nitrogen- and sulfur-containing species (e.g., O_xS_1 and N_1O_x) were also observed in oil-soluble, IM, and WSO fractions from irradiated oil, despite a low abundance of these species in the parent oil (Figs. S1, S4, and S5). The increased levels of oxidation occurring across S- and N-containing acidic classes in oil-soluble species matches the trend observed in oil-impacted salt marsh residues (field samples) from Barataria Bay (Chen et al., 2016). Parent MWO is reported to contain 0.4 wt% sulfur and 0.3 wt% nitrogen, but the sulfur content increased to 0.9 wt%, and nitrogen content remained constant for 4-year weathered oil samples collected in a Louisiana saltmarsh (Chen et al., 2016). Following solar irradiation in the microcosms, a rapid decline in the relative abundance of pyrrolic nitrogen (N_1) classes and lower-order oxygenated N_1O_x species was observed, instead of elevated levels of higher-order N_1O_x species present (Fig. S1c). After 120 h of simulated solar exposure, N_1, N_1O_1, and N_1O_2 oil-soluble species presented in the dark control microcosm were no longer detectable, whereas newly formed N_1O_4 - N_1O_8 species were observed (Figs. S1c, S6). Although the O_xS_1 species generally exhibit lower relative abundances than the O_x and N_1O_x species, consistent with the low sulfur content in the starting material, a continuum of O_3S_1 to O_8S_1 oil-soluble photoproducts from the MWO oil film is observed (Fig. S1b). Similar trends were seen for the sulfur and nitrogen species in the IM and WSO fractions (Figs. S4 and S5), in which longer irradiation periods yielded higher abundances of higher-order oxygenated N- and S-containing species (up to N_1O_{10} and $O_{10}S_1$). The results are supported by a recent study of photoproducts derived from sulfur-containing compounds from the MWO oil, where oil was separated into fractions enriched with specific sulfur chemical functionality (sulfides and thiophenic) and irradiated separately to determine the role of sulfur functionality in the formation of photoproducts from sunlight (Niles et al., 2020a). The study found abundant oil-soluble and water-soluble photoproducts in both the sulfide and thiophene fractions upon laboratory photoirradiation, regardless of their chemical functionality.

The isoabundance-contoured plots of DBE versus carbon number for the sulfur-containing photoproducts (O_xS_1) from the WSO fraction are shown in Fig. S7 and illustrate the presence of higher-oxygenated sulfur-containing compounds (O_8S_1 to $O_{12}S_1$) which form after irradiation. The dark control contains O_xS_1 (x = 1–7) species with low carbon number (<25) and DBE values (<10). However, as more oxygen atoms are incorporated with longer irradiation periods, a shift to higher aromaticity and carbon number is observed, illustrated by the dashed red circle that represents the compositional range for the O_3S_1 class at 0 h. A similar trend has been reported in the photoproducts of an asphalt binder. Most changes in the compositional space of water-soluble SO_x species were observed within the first 3 h of photoirradiation (Lalli et al., 2017).

4. Conclusions

The current study reveals a time-dependent process of how photooxidation contributes to the formation of emulsified oil/floating mats observed in the Gulf of Mexico after an oil spill through the quantified/characterized

generation of IM and to the dissolved organic carbon pool by WSO. Photoirradiation microcosm experiments conducted over a time period equivalent to 30 days of average Northern Gulf of Mexico sunlight exposure on the sea surface have demonstrated the formation of abundant oxygenated species in the oil phase, IM, and water phase. The oxygen content increases steadily from the oil-soluble to water-soluble fractions with the assistance of interfacially active species. Most compositional changes of photoproducts occurred within the first 24 h of simulated irradiation in all three fractions, indicating the importance of photochemical reactions which occur within the first four days in the environment. This suggests that photodegradation occurs within the first few hours of solar exposure, thereby mobilizing oil components into aquatic ecosystems. The most rapid change was in the water phase, where compositional differences were observed after 1 h of simulated solar exposure. The length of solar exposure also affects the bioavailability and acute toxicity per unit carbon of petroleum. Only initial water-soluble species produced within 24 h of irradiation exhibited higher toxicity relative to the dark control, with the maximum toxicity observed at 6 h (1 solar equivalent day). The increased toxicity is likely due to the structure/ chemical functionality of photoproducts formed in the early time period. Detailed temporal analysis of the phototransformation products exposed the oxygen dependence of solubility. When comparing photoproduct fractions, the oil-soluble species contain fewer oxygen atoms, become interfacially active upon further oxidation, and eventually yield water-soluble species that continuously increase the dissolved carbon pool in water. A comprehensive molecular-level understanding of the photooxidation process offers new insight into the dominant process that influences emulsion formation and changes the chemical, physical, and biological properties of the surface oil with increased exposure to solar irradiation. Because early irradiation period photoproducts are formed most rapidly, quantified reaction rates as a function of structure and mechanism (direct vs. indirect) might shed light on the increased toxicity in future studies.

CRediT authorship contribution statement

Huan Chen: Conceptualization, Methodology, Validation, Formal analysis, Investigation, Data curation, Visualization, Writing – original draft. **Amy M. McKenna**: Methodology, Validation, Writing – review & editing. **Sydney F. Niles**: Methodology, Formal analysis, Writing – review & editing. **Joseph W. Frye**: Methodology, Writing – review & editing. **Taylor J. Glattke**: Methodology, Writing – review & editing. **Ryan P. Rodgers**: Conceptualization, Methodology, Investigation, Validation, Formal analysis, Funding acquisition, Writing – review & editing.

Declaration of competing interest

The authors declare that they have no known competing financial interests or personal relationships that could have appeared to influence the work reported in this paper.

Acknowledgements

Work performed at the National High Magnetic Field Laboratory ICR Facility is supported by the National Science Foundation Division of Materials Research and Division of Chemistry through DMR 1644779, the State of Florida, and in part by a grant from The Gulf of Mexico Research Initiative. Data are publicly available through the Gulf of Mexico Research Initiative Information & Data Cooperative (GRIIDC) at https://data.gulfresearchinitiative.org (https://doi.org/10.7266/F30JSDGR). We thank Sarajeen Saima Hoque for the DOC measurement.

Appendix A. Supplementary data

Supplementary data to this article can be found online at https://doi.org/10.1016/j.scitotenv.2021.151884.

References

Aeppli, C., Carmichael, C.A., Nelson, R.K., Lemkau, K.L., Graham, W.M., Redmond, M.C., Valentine, D.L., Reddy, C.M., 2012. Oil weathering after the Deepwater Horizon disaster led to the formation of oxygenated residues. Environ. Sci. Technol. 46 (16), 8799–8807.

Ali, L.N., Mantoura, R.F., Rowland, S.J., 1995. The dissolution and photodegradation ofKuwaiti crude oil in seawater. Part 2: a laboratory photodegradation apparatus and photodegradation kinetics of a model seawater soluble hydrocarbon(phenanthrene). Mar. Environ. Res. 40, 319–335.

Bacosa, H.P., Erdner, D.L., Liu, Z., 2015. Differentiating the roles of photooxidation and biodegradation in the weathering of Sight Louisiana Sweet crude oil in surface water from the Deepwater Horizon site. Mar. Pollut. Bull. 95 (1), 265–272.

Barron, M.G., 2017. Photoenhanced toxicity of petroleum to aquatic invertebrates and fish. Arch. Environ. Contam. Toxicol. 73 (1), 40–46.

Barron, M.G., Carls, M.G., Short, J.W., Rice, S.D., 2003. Photoenhanced toxicity of aqueous phase and chemically dispersed weathered Alaska North Slope crude oil to Pacific herring eggs and larvae. Environ. Toxicol. Chem. 22 (3), 650–660.

Brohon, B., Delolme, C., Gourdon, R., 2001. Complementarity of bioassays and microbial activity measurements for the evaluation of hydrocarbon-contaminated soils quality. Soil Biol. Biochem. 33 (7), 883–891.

Chen, H., Hou, A., Corilo, Y.E., Lin, Q., Lu, J., Mendelssohn, I.A., Zhang, R., Rodgers, R.P., McKenna, A.M., 2016. 4 years after the Deepwater Horizon spill: molecular transformation of Macondo well oil in Louisiana salt marsh sediments revealed by FT-ICR mass spectrometry. Environ. Sci. Technol. 50 (17), 9061–9069.

Chen, H., Nelson, R.K., Swarthout, R.F., Shigenaka, G., de Oliveira, A.H., Reddy, C.M., McKenna, A.M., 2018. Detailed compositional characterization of the 2014 Bangladesh furnace oil released into the world's largest mangrove forest. Energy Fuel 32 (3), 3232–3242.

Clingenpeel, A.C., Robbins, W.K., Corilo, Y.E., Rodgers, R.P., 2015. Effect of the water content on silica gel for the isolation of interfacial material from Athabasca bitumen. Energy Fuel 29 (11), 7150–7155.

Corilo, Y.E., Podgorski, D.C., McKenna, A.M., Lemkau, K.L., Reddy, C.M., Marshall, A.G., Rodgers, R.P., 2013. Oil spill source identification by principal component analysis of electrospray ionization Fourier transform ion cyclotron resonance mass spectra. Anal. Chem. 85 (19), 9064–9069.

Daling, P.S., Leirvik, F., Almås, I.K., Brandvik, P.J., Hansen, B.H., Lewis, A., Reed, M., 2014. Surface weathering and dispersibility of MC252 crude oil. Mar. Pollut. Bull. 87 (1–2), 300–310.

Dittmar, T., Koch, B., Hertkorn, N., Kattner, G., 2008. A simple and efficient method for the solid-phase extraction of dissolved organic matter (SPE-DOM) from seawater. Limnol. Oceanogr. Methods 6 (6), 230–235.

Dutta, T.K., Haryama, S., 2000. Fate of crude oil by the combination of photoxidation and biodegradation. Environ. Sci. Technol. 34, 264–269.

Echols, B.S., Smith, A.J., Gardinali, P.R., Rand, G.M., 2015. Acute aquatic toxicity studies of Gulf of Mexico water samples collected following the Deepwater Horizon incident (May 12, 2010 to December 11, 2010). Chemosphere 120, 131–137.

Faksness, L.G., Altin, D., Nordtug, T., Daling, P.S., Hansen, B.H., 2015. Chemical comparison and acute toxicity of water accommodated fraction (WAF) of source and field collected Macondo oils from the Deepwater Horizon spill. Mar. Pollut. Bull. 91 (1), 222–229.

Fernandez-Varela, R., Gomez-Carracedo, M.P., Fresco-Rivera, P., Andrade, J.M., Muniategui, S., Prada, D., 2006. Monitoring photooxidation of the Prestige's oil spill byattenuated total reflectance infrared spectroscopy. Talanta 69, 409–417.

Garrett, R.M., Pickering, I.J., Haith, C.E., Prince, R.C., 1998. Photooxidation of crude oils. Environ. Sci. Technol. 32, 3719–3723.

Gough, M.A., Rowland, S.J., 1990. Characterization of unresolved complex mixtures of hydrocarbons in petroleum. Nature 344, 648–650.

Gros, J., Reddy, C.M., Aeppli, C., Nelson, R.K., Carmichael, C.A., Arey, J.S., 2014. Resolving biodegradation patterns of persistent saturated hydrocarbons in weathered oil samples from the Deepwater Horizon disaster. Environ. Sci. Technol. 48 (3), 1628–1637.

Guipeng, Y., Li, Z., Xiaojing, S., Weiwen, J., 2006. Photochemical degradation of crude oil in seawater. Chin. J. Oceanol. Limnol. 24, 264–269.

Harriman, B.H., Zito, P., Podgorski, D.C., Tarr, M.A., Suflita, J.M., 2017. Impact of photooxidation and biodegradation on the fate of oil spilled during the Deepwater Horizon incident: advanced stages of weathering. Environ. Sci. Technol. 51 (13), 7412–7421.

Jarvis, J.M., Robbins, W.K., Corilo, Y.E., Rodgers, R.P., 2015. Novel method to isolate interfacial material. Energy Fuel 29 (11), 7058–7064.

Johnson, B.T., 2018. Microtox® toxicity test system—new developments and applications. Microscale Testing in Aquatic Toxicology. CRC Press, pp. 201–218.

Kaiser, N.K., Quinn, J.P., Blakney, G.T., Hendrickson, C.L., Marshall, A.G., 2011. A novel 9.4 Tesla FT ICR mass spectrometer with improved sensitivity, mass resolution, and mass range. J. Am. Soc. Mass Spectrom. 22 (8), 1343–1351.

Kim, S., Kramer, R.W., Hatcher, P.G., 2003. Graphical method for analysis of ultrahigh-resolution broadband mass spectra of natural organic matter, the van Krevelen diagram. Anal. Chem. 75 (20), 5336–5344.

King, S.M., Leaf, P.A., Olson, A.C., Ray, P.Z., Tarr, M.A., 2014. Photolytic and photocatalytic degradation of surface oil from the Deepwater Horizon spill. Chemosphere 95, 415–422.

Kujawinski, E.B., Reddy, C.M., Rodgers, R.P., Thrash, J.C., Valentine, D.L., White, H.K., 2020. The first decade of scientific insights from the Deepwater Horizon oil release. Nat. Rev. Earth Environ. 1 (5), 237–250.

Lalli, P.M., Jarvis, J.M., Marshall, A.G., Rodgers, R.P., 2017. Functional isomers in petroleum emulsion interfacial material revealed by ion mobility mass spectrometry and collision-induced dissociation. Energy Fuel 31 (1), 311–318.

Lee, R.F., 2003. Photo-oxidation and photo-toxicity of crude and refined oils. Spill Sci. Technol. Bull. 8 (2), 157–162.

Lee, K., Wohlgeschaffen, G., Thomas Johnson, B., Sergy, G.A., Prince, R.C., Guénette, C.C., Owens, E.H., Tremblay, G.H., 2003. Toxicity evaluation with the microtox® test to assess the impact of in situ oiled shoreline treatment options: natural attenuation and sediment relocation. Spill Sci. Technol. Bull. 8 (3), 273–284.

Lelario, F., Bianco, G., Bufo, S.A., Scrano, L., 2021. Simulated ageing of crude oil and advanced oxidation processes for water remediation since crude oil pollution. Catalysts 11 (8), 954.

Lewan, M., Warden, A., Dias, R., Lowry, Z., Hannah, T., Lillis, P., Kokaly, R., Hoefen, T., Swayze, G., Mills, C., 2014. Asphaltene content and composition as a measure of Deepwater Horizon oil spill losses within the first 80 days. Org. Geochem. 75, 54–60.

Lobodin, V.V., Juyal, P., McKenna, A.M., Rodgers, R.P., Marshall, A.G., 2013. Tetramethylammonium hydroxide as a reagent for complex mixture analysis by negative ion electrospray ionization mass spectrometry. Anal. Chem. 85 (16), 7803–7808.

Maki, H., Sasaki, T., Harayama, S., 2001. Photo-oxidation of biodegraded crude oil and toxicity of the photo-oxidized products. Chemosphere 44 (5), 1145–1151.

McKenna, A.M., Nelson, R.K., Reddy, C.M., Savory, J.J., Kaiser, N.K., Fitzsimmons, J.E., Marshall, A.G., Rodgers, R.P., 2013. Expansion of the analytical window for oil spill characterization by ultrahigh resolution mass spectrometry: beyond gas chromatography. Environ. Sci. Technol. 47 (13), 7530–7539.

Morales-Caselles, C., Kalman, J., Riba, I., DelValls, T., 2007. Comparing sediment quality in Spanish littoral areas affected by acute (Prestige, 2002) and chronic (Bay of Algeciras) oil spills. Environ. Pollut. 146 (1), 233–240.

Murray, J.A., Murray, J.A., Reddy, C.M., Sander, L.C., Wise, S.A., 2016. Gulf of Mexico Research Initiative 2014/2015 Hydrocarbon Intercalibration Experiment: Description and Results for SRM 2779 Gulf of Mexico Crude Oil and Candidate SRM 2777 Weathered Gulf of Mexico Crude Oil. US Department of Commerce, National Institute of Standards and Technology.

Niles, S.F., Chacón-Patiño, M.L., Chen, H., McKenna, A.M., Blakney, G.T., Rodgers, R.P., Marshall, A.G., 2019. Molecular-level characterization of oil-soluble ketone/aldehyde photo-oxidation products by Fourier transform ion cyclotron resonance mass spectrometry reveals similarity between microcosm and field samples. Environ. Sci. Technol. 53 (12), 6887–6894.

Niles, S.F., Chacón-Patiño, M.L., Marshall, A.G., Rodgers, R.P., 2020. Molecular composition of photooxidation products derived from sulfur-containing compounds isolated from petroleum samples. Energy Fuel 34 (11), 14493–14504.

Niles, S.F., Chacón-Patiño, M.L., Putnam, S.P., Rodgers, R.P., Marshall, A.G., 2020. Characterization of an asphalt binder and photoproducts by Fourier transform ion cyclotron resonance mass spectrometry reveals abundant water-soluble hydrocarbons. Environ. Sci. Technol. 54 (14), 8830–8836.

Passow, U., Overton, E.B., 2021. The complexity of spills: the fate of the Deepwater Horizon oil. Annu. Rev. Mar. Sci. 13, 109–136.

Pelletier, E., Delille, D., Delille, B., 2004. Crude oil bioremediation in sub-Antarctic intertidal sediments: chemistry and toxicity of oiled residues. Mar. Environ. Res. 57 (4), 311–327.

Radović, J.R., Aeppli, C., Nelson, R.K., Jimenez, N., Reddy, C.M., Bayona, J.M., Albaigés, J., 2014. Assessment of photochemical processes in marine oil spill fingerprinting. Mar. Pollut. Bull. 79 (1–2), 268–277.

Radović, J.R., Jaggi, A., Silva, R.C., Snowdon, R., Waggoner, D.C., Hatcher, P.G., Larter, S.R., Oldenburg, T.B., 2020. Applications of FTICR-MS in oil spill studies. Deep Oil Spills. Springer, pp. 253–268.

Ray, P.Z., Tarr, M.A., 2014. Petroleum films exposed to sunlight produce hydroxyl radical. Chemosphere 103, 220–227.

Reddy, C.M., Arey, S.J., Seewald, J.S., Sylva, S.P., Lemkau, K.L., Nelson, R.K., Carmichael, C.A., McIntyre, C.P., Fenwick, J., Ventura, G.T., 2011. Composition and fate of gas and oil released to the water column during the Deepwater Horizon oil spill. Proc. Nat. Acad. Sci. 1–6 Early Edition.

Roebuck Jr., J.A., Podgorksi, D.C., Wagner, S., Jaffé, R., 2017. Photodissolution of charcoal and fire-impacted soil as a potential source of dissolved black carbon in aquatic environments. Org. Geochem. 112, 16–21.

Ruddy, B.M., Huettel, M., Kostka, J.E., Lobodin, V.V., Bythell, B.J., McKenna, A.M., Aeppli, C., Reddy, C.M., Nelson, R.K., Marshall, A.G., 2014. Targeted petroleomics: analytical investigation of Macondo well oil oxidation products from Pensacola Beach. Energy Fuel 28 (6), 4043–4050.

Seidel, M., Kleindienst, S., Dittmar, T., Joye, S.B., Medeiros, P.M., 2016. Biodegradation of crude oil and dispersants in deep seawater from the Gulf of Mexico: insights from ultrahigh resolution mass spectrometry. Deep-Sea Res. II Top. Stud. Oceanogr. 129, 108–118.

Sleighter, R.L., Hatcher, P.G., 2008. Molecular characterization of dissolved organic matter (DOM) along a river to ocean transect of the lower Chesapeake Bay by ultrahigh resolution electrospray ionization Fourier transform ion cyclotron resonance mass spectrometry. Mar. Chem. 110 (3–4), 140–152.

Stout, S.A., Payne, J.R., Emsbo-Mattingly, S.D., Baker, G., 2016. Weathering of field-collected floating and stranded Macondo oils during and shortly after the Deepwater Horizon oil spill. Mar. Pollut. Bull. 105 (1), 7–22.

Thingstad, T., Pengerud, B., 1983. The formation of “chocolate mousse” from statfjord crude oil and seawater. Mar. Pollut. Bull. 14 (6), 214–216.

Vaughan, P.P., Wilson, T., Kamerman, R., Hagy, M.E., McKenna, A., Chen, H., Jeffrey, W.H., 2016. Photochemical changes in water accommodated fractions of MC252 and surrogate oil created during solar exposure as determined by FT-ICR MS. Mar. Pollut. Bull. 104 (1–2), 262–268.

Vione, D., Minella, M., Maurino, V., Minero, C., 2014. Indirect photochemistry in sunlit surface waters: photoinduced production of reactive transient species. Chem. Eur. J. 20 (34), 10590–10606.

Ward, C.P., Overton, E.B., 2020. How the 2010 Deepwater Horizon spill reshaped our understanding of crude oil photochemical weathering at sea: a past, present, and future perspective. Environ. Sci. Process. Impacts 22 (5), 1125–1138.

Ward, C.P., Sharpless, C.M., Valentine, D.L., French-McCay, D.P., Aeppli, C., White, H.K., Rodgers, R.P., Gosselin, K.M., Nelson, R.K., Reddy, C.M., 2018. Partial photochemical oxidation was a dominant fate of Deepwater Horizon surface oil. Environ. Sci. Technol. 52 (4), 1797–1805.

Zhou, Z., Liu, Z., Guo, L., 2013. Chemical evolution of macondo crude oil during laboratory degradation as characterized by fluorescence EEMs and hydrocarbon composition. Mar. Pollut. Bull. 66 (1), 164–175.

Zito, P., Podgorski, D.C., Johnson, J., Chen, H., Rodgers, R.P., Guillemette, F., Kellerman, A.M., Spencer, R.G., Tarr, M.A., 2019. Molecular-level composition and acute toxicity of photosolubilized petrogenic carbon. Environ. Sci. Technol. 53 (14), 8235–8243.

Zito, P., Podgorski, D.C., Bartges, T., Guillemette, F., Roebuck Jr., J.A., Spencer, R.G., Rodgers, R.P., Tarr, M.A., 2020. Sunlight-induced molecular progression of oil into oxidized oil soluble species, interfacial material, and dissolved organic matter. Energy Fuel 34 (4), 4721–4726.